PHYSICAL REVIEW C **76**, 011603(R) (2007)

Baryon deceleration by strong chromofields in ultrarelativistic nuclear collisions

Igor N. Mishustin[1,2] and Konstantin A. Lyakhov[3]
[1]*Frankfurt Institute for Advanced Studies, J.W. Goethe University, D-60438 Frankfurt am Main, Germany*
[2]*The Kurchatov Institute, Russian Research Center, RU-123182 Moscow, Russia*
[3]*Frankfurt International Graduate School for Science, J.W. Goethe University, D-60438 Frankfurt am Main, Germany*
(Received 11 December 2006; published 26 July 2007)

It is assumed that strong chromofields are generated at early stages of ultrarelativistic heavy-ion collisions which give rise to a collective deceleration of baryons from colliding nuclei. We have solved classical equations of motion for baryonic slabs under the action of a time-dependent longitudinal chromoelectric field. It is demonstrated that the slab final rapidities are rather sensitive to the strength and decay time of the chromofield as well as to the back reaction of the produced partonic plasma. The net-baryon rapidity loss $\langle \delta y \rangle = 2.0$, found for most central Au-Au collisions at RHIC, can be explained by the action of chromofields with the initial energy density of about 50 GeV/fm^3. Predictions of the baryon stopping for the LHC energy are made.

DOI: 10.1103/PhysRevC.76.011603 PACS number(s): 25.75.−q, 12.38.Mh, 24.10.Jv, 24.85.+p

It is expected that strong chromofields can develop at early stages of ultrarelativistic heavy-ion collisions. There exist different suggestions concerning the space-time structure of these fields, ranging from string-like configurations as in the color flux tube model (FTM) [1] to stochastic configurations associated with the color glass condensate (CGC) [2]. This picture is most conveniently presented in the c.m. frame where two Lorentz contracted nuclei look as thin sheets. After their intersection these sheets acquire stochastic color charges as a result of multiple soft gluon exchange. Then strong chromofields are generated in the space between the receding sheets. At later times these fields decay into quarks and gluons which after equilibration form a quark-gluon plasma. This process has been studied by several authors under different assumptions about the field decay mechanism (see, e.g., Refs. [3–5]).

Most previous calculations assume that after interaction the nuclear debris follow the light-cone trajectories, thus disregarding their energy losses to produce the chromofield. This assumption can possibly be justified only at asymptotically high energies. Furthermore, this assumption becomes irrelevant when studying the baryon stopping. Obviously, the energy of produced fields and particles is taken entirely from the kinetic energy of the colliding nuclei.

As measured by the BRAHMS collaboration [6], in central Au+Au collisions at highest RHIC energy $\sqrt{s_{NN}} = 200$ GeV per NN-pair the baryon energy losses are very significant, about 70% of the initial energy. The measured net-baryon rapidity distributions show significant population of the central rapidity region.

The problem of baryon stopping at RHIC has been addressed recently by several authors. In particular, net-baryon rapidity distributions were calculated within the microscopic string-based models like URQMD [7] and QGSM [8]. Although these models implement energy and momentum conservation, and thus predict a certain baryon stopping, they are formulated in momentum space and do not give a space-time picture of this process. Also, they are dealing with hadronic secondaries and therefore preclude the quark-gluon plasma formation. Recently, the calculations have been done within a parton cascade model [9]. The distribution of valence quarks at central rapidities was also studied in Ref. [10] within a QCD motivated approach which however can not be extended to the fragmentation regions.

In Ref. [11] a simple space-time model was proposed where the baryon stopping was directly linked to the formation of strong chromofields. There nuclear trajectories were calculated under assumption that the field is neutralized at a sharp proper time 1 fm/c (see also Refs. [12,13]). In this Rapid Communication we further develop this model and apply it for a more realistic decay pattern of the chromofield. Our main goal is to calculate the net-baryon rapidity distribution and compare it with the BRAHMS data.

Following Ref. [14] we decompose the collision of two ultrarelativistic nuclei into a set of pairwise collisions of elementary slabs. At given impact parameter **b** the positions of the colliding target and projectile slabs in the transverse plane are determined by vectors **s** and **b** − **s**, respectively. The cross section area of individual slabs, σ_0, is a model parameter which determines the coarse-graining scale in the transverse plane. It should be larger than the cross section of individual flux tubes (about 0.2 fm^2), and smaller than the total transverse area of the overlap zone. In numerical calculations we choose it equal to the nucleon-nucleon inelastic cross section, $\sigma_0 = \sigma_{NN} \approx 4$ fm^2. This corresponds to the picture when many string-like field configurations are stretched between the receding slabs. Final results are not very sensitive to this parameter.

The energy and momentum of the projectile ($a = p$) and target($a = t$) slabs are parameterized as $E_a = M_a \cosh Y_a$ and $P_a = M_a \sinh Y_a$, where $M_a = m_\perp N_a$ is the average transverse mass and N_a is the average baryon number of slab a. The average baryon transverse mass $m_\perp$ differs from the free nucleon mass m_N due to internal excitation of slabs. It is expressed as $m_\perp = \sqrt{m_N^2 + \langle p_\perp \rangle^2}$, where the mean transverse momentum $\langle p_\perp \rangle$ is in general a function of time. The calculations below are made in light-cone coordinates, proper time $\tau = \sqrt{t^2 - z^2}$ and space-time rapidity $\eta = \frac{1}{2} \ln(\frac{t+z}{t-z})$.

In the Glauber model (see, e.g., Refs. [15,16]) the average number of participating nucleons from nucleus a in a slab of

transverse area σ located at a radius-vector $\mathbf{s}$ is given by the expression

$$N_a(\mathbf{b},\mathbf{s}) = \sigma_{NN} A_a T_a(\mathbf{b}-\mathbf{s})(1-[1-\sigma_{NN} T_{\bar{a}}(\mathbf{s})]^{A_{\bar{a}}}), \quad (1)$$

where $\bar{a} = t$ for $a = p$ and vice versa, A_a is the mass number of nucleus a. The normalized functions T_a $(a = p, t)$ describe the transverse profiles of the baryon number distribution in colliding nuclei. They are obtained by the integration of the corresponding baryon densities along the beam direction, $A_a T_a = \int \rho_a(\mathbf{r}) dz$. The average number of nucleon-nucleon collisions in an inelastic interaction of two slabs at a radius-vector $\mathbf{s}$ is expressed as

$$N_{\rm coll}(\mathbf{b},\mathbf{s}) = \sigma_{NN}^2 A_p T_p(\mathbf{b}-\mathbf{s}) A_t T_t(\mathbf{s}) \approx N_p(\mathbf{b},\mathbf{s}) N_t(\mathbf{b},\mathbf{s}). \quad (2)$$

We assume that the initial energy density stored in the chromofield after collision of two baryonic slabs can be parametrized as

$$\epsilon_f(\tau_0;\mathbf{b},\mathbf{s}) = \epsilon_0 \left(\frac{s}{s_0}\right)^{\alpha} [N_{\rm coll}(\mathbf{b},\mathbf{s})]^{\beta}, \quad (3)$$

where ϵ_0 is the model parameter, which can be determined by comparison with experimental data. The second factor describes the collision energy dependence with $\alpha \approx 0.3$, as motivated by small x behavior of the gluon structure function [17]. The last factor describes effects of the collision geometry, where exponent β is related to the spatial distribution of the chromofield. For nonoverlapping strings $\beta \approx 1.0$, but in the case of string clustering β is expected to be closer to 0.5 [18]. In this paper we consider only the case $\beta = 1$.

We assume that the space between the receding slabs is occupied by the chromofield and a partonic plasma, produced by the partial field decay. They exert certain forces on the slab from inside, in particular, the Lorentz force acting on the color charges generated on the slab. But from the other side the slab has nothing but the physical vacuum. This results in a net force leading to the slab deceleration. The equations of motion for for individual slabs can be obtained by applying the energy-momentum conservation laws across the slab. The final system of differential equations governing the slab rapidities $Y_a(\tau)$ has the following form (detailed calculations see in Ref. [19]):

$$\frac{d\tilde{P}_a}{d\tau} = \mp B(\tau) - \frac{\tilde{P}_a}{\tau}, \quad (4)$$

$$\frac{dM_a^2}{d\tau} = \mp 2A(\tau)\tilde{P}_a, \quad (5)$$

$$\frac{d\eta_a}{d\tau} = \mp \frac{\tilde{P}_a}{\tau \tilde{E}_a}, \quad (6)$$

where $\tilde{P}_a = M_a \sinh(Y_a - \eta_a)$, $\tilde{E}_a = \sqrt{M_a^2 + \tilde{P}_a^2}$, $B(\tau) = \sigma_{NN}(\epsilon_{vac} + \epsilon_f - p)$, and $A(\tau) = \sigma_{NN}(\epsilon_p + p)$. The plus and minus signs in the right hand side of these equations correspond to the projectile $(a = p)$ and target $(a = t)$ slabs, respectively. We adopt the initial conditions for the slab trajectories $\eta_a(\tau_0) = Y_a(\tau_0) = \pm y_0$ at $\tau_0 \approx 0$, where $\pm y_0$ are the initial c.m. rapidities of colliding nuclei. In expressions above ϵ_p and $p = c_s^2 \epsilon_p$ are, respectively, the energy density and pressure of the partonic plasma, and c_s is the corresponding sound velocity. The vacuum energy density ϵ_{vac} (bag constant) is introduced to account for the fact that the chromofield and partonic plasma can exist only in the perturbative vacuum. In numerical calculations ϵ_{vac} is fixed to the value 0.4 GeV/fm^3. It is assumed that the chromofield energy density $\epsilon_f(\tau)$ and the plasma energy density $\epsilon_p(\tau)$ are functions of the proper time τ only, defined in the interval $\eta_t(\tau) \leqslant \eta \leqslant \eta_p(\tau)$. Then the partonic plasma has a Bjorken-like velocity field, $v = \tanh\eta$ [20]. The plasma energy density, $\epsilon_p(\tau)$ is found from the hydrodynamical equation with a source term due to the field decay:

$$\frac{d\epsilon_p}{d\tau} + (1 + c_s^2)\frac{\epsilon_p}{\tau} = -\frac{d\epsilon_f}{d\tau}. \quad (7)$$

We integrate Eqs. (4)–(6) until the time when the total pressure in the region between the slabs vanishes, i.e., $B(\tau) = 0$. After this time the slabs move with constant velocity. Obviously, the solution of Eq. (4) is

$$\tilde{P}_a = \tilde{P}_a(\tau_0)\frac{\tau_0}{\tau} \mp \frac{1}{\tau}\int_{\tau_0}^{\tau} B(\tau)\tau d\tau, \quad (8)$$

and the slab rapidity $Y_a(\tau)$ can be easily found from the definition $\tilde{P}_a = M_a \sinh(Y_a - \eta_a)$. Then, the slab trajectory, $z_a(\tau)$, is obtained from the relation $z_a = \tau \sinh\eta_a$.

Below we present results for Au+Au and d+Au collisions at maximum RHIC energy $\sqrt{s_{NN}} = 200$ GeV per NN pair $(y_0 = 5.4)$. The nucleon-nucleon inelastic cross section was taken to be $\sigma_{NN} = 42$ mb [16]. The baryon mean transverse momentum $\langle p_\perp \rangle$ is constrained by the value around 1.0 GeV/c, as measured by the BRAHMS collaboration [6].

We have considered several functional forms for the time dependence of the chromofield, resulting in different plasma production rates and baryon deceleration patterns. Here we present results for the power law, $\epsilon_f(\tau) = \epsilon_f(\tau_0)[1 + \frac{\tau-\tau_0}{\tau_d}]^{-4}$ characterized by the decay time $\tau_d = 0.6$ fm/c, as expected for the Schwinger-like decay mechanism [3]. This function is shown in Fig. 1 together with the time dependence of the plasma energy density as predicted by the hydrodynamical equation (7) with $c_s^2 = 1/3$. According to our picture, the quark-gluon plasma (QGP) is produced by the continuous transformation of the field energy into the quark-antiquark and gluon pairs. Because of the delayed production, the plasma energy density is always smaller than the initial energy density of the chromofield. In accordance with previous calculations [3], we find that it reaches only about 22% of the latter for the Schwinger-like decay law.

Figure 2 shows how the time evolution of the slab rapidities $Y_{p,t}(\tau)$ depends on the initial energy density of the chromofield, as well as on the baryon numbers of colliding slabs. We present results for several values of the parameter ϵ_0 [see Eq. (3)] between 1.0 and 3.0 GeV/fm^3. Upper panels show results for the collision of two equal slabs with baryon numbers $N_p = N_t = 5.7$, representing an average pair of slabs in a central Au+Au collision. The initial energy densities of the chromofield, $\epsilon_f(\tau_0)$, range in this case from 33 (lower curves) to 100 (upper curves) GeV/fm^3. According to the BRAHMS data [6] the mean baryon rapidity loss for the most central Au-Au collisions is $\langle \delta y \rangle \approx 2.0$. From the figures

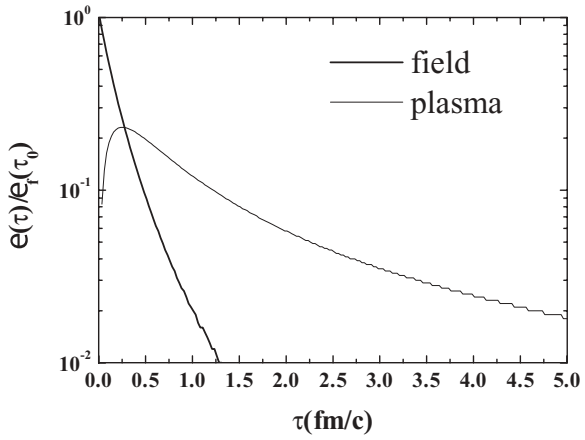

FIG. 1. Evolution of the chromofield energy density (thick solid line) and QGP energy density (thin solid line) in units of the initial chromofield energy density $\epsilon_f(\tau_0)$. Results are shown for the Schwinger-like (power-law) decay mechanism with $\tau_d = 0.6$ fm/c.

one can see that slab rapidities $Y_{p,t}(\tau)$ drop rapidly at very early stages of the deceleration process, when the field is still strong. At later times, not only the decreasing chromofield (see Fig. 1) but also the plasma counter-pressure (left panels) cause an early termination of the deceleration process. As the result, the asymptotic slab rapidities have a low sensitivity to the initial chromofield energy density. Nevertheless, the observed rapidity loss can be achieved with the initial field energy density $\epsilon_f(\tau_0) = 60$–80 GeV/fm^3. On the other hand, due to the edge effects, the plasma pressure in the vicinity of the slabs should be smaller than in the central region. Then the deceleration process will be less affected by the plasma, and resulting slabs' rapidities will be smaller. This is illustrated in the right panels showing calculations of the slab rapidities ignoring the plasma pressure. In this case the required rapidity loss can be achieved with a much weaker chromofield, $\epsilon_f(\tau_0) \approx 20$–$40$ GeV/fm^3. It is clear that the realistic situation will be in between of these two extremes.

Low panels show results for an asymmetric collision of $N_p = 2$ and $N_t = 8.8$ slabs, which can be interpreted as a deuteron colliding with a center of a gold nucleus. The parameter ϵ_0 is the same as before but now it corresponds to $\epsilon_f(\tau_0)$ between 8.9 and 35.5 GeV/fm^3. One can see that the rapidity shifts are now different for the light and heavy slabs. Moreover, the rapidity lost by the smaller slab is significantly larger as compared with the bigger one. This is of course a direct consequence of the fact that equal forces generate a larger deceleration for a smaller body.

According to the CGC picture [2,4], the color charge fluctuates the Gaussian weights with mean value equal to zero and variance given by the model parameter μ^2. In a flux-tube configuration the chromoelectric field is proportional to the areal charge density at the slab spot to which the tube is attached. The corresponding field energy density is proportional to the square of the areal charge density. Therefore, in terms of the field energy density the weights are exponential, i.e., $P(\epsilon_f) \propto \exp[-\frac{\epsilon_f}{\langle\epsilon_f\rangle}]$, where $\langle\epsilon_f\rangle \equiv \epsilon_f(\tau_0)$ is the mean energy density of the field parametrized in Eq. (3). When many string-like configurations are stretched between the slabs, the resulting force is the sum of many fluctuating contributions. It is easy to show [19] that it obeys a so-called gamma-distribution. This distribution looks like an asymmetric Gaussian with a long tail at large arguments. Figure 3 shows the calculated and measured net-baryon rapidity distributions for most central Au+Au collisions at maximum RHIC energy. The introduction of the field fluctuations leads to an interesting effect: since stronger fields lead to larger decelerations of the slabs, the resulting net-baryon rapidity distribution acquires a long tail toward central rapidities. This is exactly what is observed by the BRAHMS collaboration [6]. Our analysis shows that this shape of the distribution cannot be reproduced with any fixed value of the field.

The rapidity spectra shown in Fig. 3 contain effect of thermal smearing corresponding to ± 0.5 units of rapidity. No back reaction of the partonic plasma on the slab deceleration

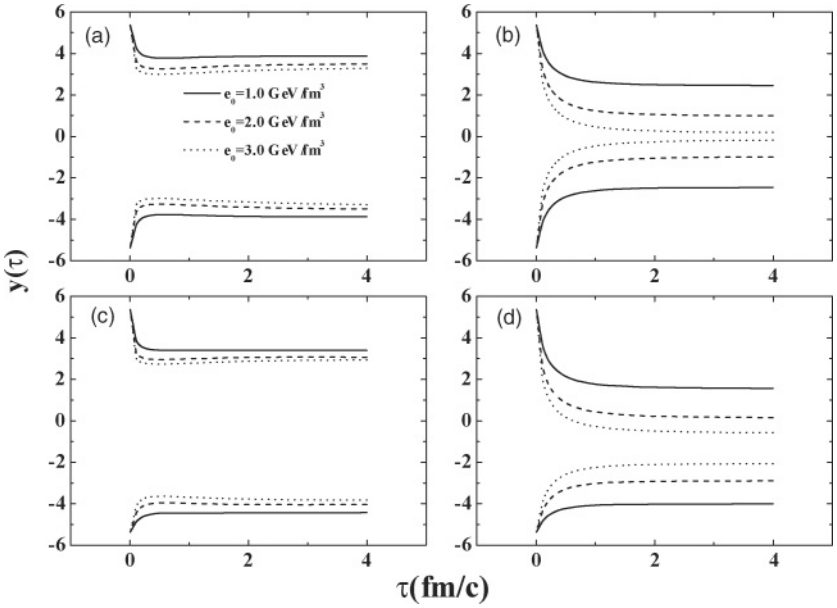

FIG. 2. Projectile (upper curves) and target (lower curves) slab rapidities as functions of proper time calculated for the power-law chromofield decay with $\tau_d = 0.6$ fm/c. Different pairs of curves correspond to different values of the parameter ϵ_0 introduced in Eq. (3). Results are shown for two cases: (a),(b) equal slabs with $N_p = N_t = 5.7$ representing a central Au+Au collision, and (c),(d) two different slabs with $N_p = 2$, $N_t = 8.8$ representing a central d+Au collision. Left and right panels show the calculations with and without the back reaction of the produced plasma, respectively.

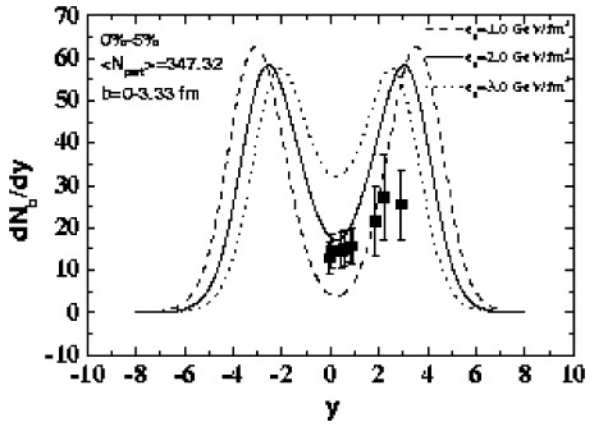

FIG. 3. Net-baryon rapidity distribution in central Au+Au collisions ($N_{\rm part} = 380$) at $\sqrt{s_{NN}} = 200$ GeV calculated for fluctuating chromofields with mean values characterized by parameter ϵ_0 as explained in the text. Back reaction of the partonic plasma is not included in the calculation of the slab rapidities. Dots are experimental data of BRAHMS collaboration [6].

was included. As one can see, in this case we can get a reasonable fit of the data with $\epsilon_0 \approx 1$–2 GeV/fm^3, which correspond to the mean values of the initial chromofield energy density in the range 40–80 GeV/fm^3. Then, according to Fig. 1, the mean energy density of the partonic plasma at $\tau = 1$ fm/c is predicted in the range of 4–8 GeV/fm^3. These values agree well with estimates based on a hydrodynamic description of the hadronic rapidity spectra at midrapidity (see, e.g., Ref. [21]).

On the basis of our model we can make predictions of the net-baryon rapidity shifts for the future LHC experiments. We use Eq. (3) to extrapolate the initial field energy densities from the RHIC ($\sqrt{s_0} = 200$ GeV) to the LHC ($\sqrt{s} = 5500$ GeV) energy domain. Then we get the mean net-baryon rapidity loss between 2.7 and 5.5 units for the calculation with and without the back reaction of partonic plasma, respectively.

In conclusion, the collective deceleration of valence (net) baryons was studied assuming that strong longitudinal chromofields are formed at early stages of an ultrarelativistic heavy-ion collision. We have solved classical equations of motion for baryonic slabs under the action of a time-dependent chromoelectric field. It has been demonstrated that the net-baryon rapidity loss $\langle \delta y \rangle \approx 2$ can be achieved with the mean energy density of the chromofield in the range of 40 to 80 GeV/fm^3. The calculated net baryon rapidity distributions for central Au+Au collisions at RHIC energies are in good agreement with BRAHMS data. The mean net-baryon rapidity loss for central Pb+Pb collisions at LHC energies is predicted between 2.7 and 5.5 units.

More detailed results, including the rapidity densities of net baryons and partonic plasma, calculated for different field decay patterns and centrality classes, will be presented in the forthcoming publication [19].

The authors thank C. Greiner, M. Gyulassy, L. McLerran, L.M. Satarov and H. Stöcker for useful discussions. This work was supported in part by the DFG grant 436RUS 113/711/0-2 (Germany), and grants RFFR-05-02-04013 and NS-8756.2006.2 (Russia).

[1] A. Casher, H. Neuberger, and S. Nussinov, Phys. Rev. D **20**, 179 (1979); N. K. Glendenning and T. Matsui, Nucl. Phys. **B245**, 449 (1984); K. Kajantie and T. Matsui, Phys. Lett. **B164**, 373 (1985); M. Gyulassy and A. Iwazaki, *ibid.* **B165**, 157 (1985).

[2] L. McLerran and R. Venugopalan, Phys. Rev. D **49**, 2233 (1994); **49**, 3352 (1994); E. Jancu and L. McLerran, Phys. Lett. **B510**, 145 (2000); L. McLerran, Nucl. Phys. **A699**, 73c (2002).

[3] G. Gatoff, A. K. Kerman, and T. Matsui, Phys. Rev. D **36**, 114 (1987); K. J. Eskola and M. Gyulassy, Phys. Rev. C **47**, 2329 (1993).

[4] A. Kovner, L. McLerran, and H. Weigert, Phys. Rev. D **52**, 3809 (1995); **52**, 6231 (1995).

[5] F. Gelis, K. Kajantie, and T. Lappi, Phys. Rev. C **71**, 024904 (2005).

[6] I. G. Bearden (BRAHMS Collaboration), Phys. Rev. Lett. **93**, 102301 (2004).

[7] S. A. Bass *et al.*, Prog. Part. Nucl. Phys. **41**, 225 (1998).

[8] N. S. Amelin, N. Armesto, C. Pajares, and D. Sousa, Eur. Phys. J. C **22**, 149 (2001).

[9] S. A. Bass, B. Müller, and D. K. Srivastava, Phys. Rev. Lett. **91**, 052302 (2005).

[10] K. Itakura, Yu. Kovchegov, L. McLerran, and D. Teaney, Nucl. Phys. **A730**, 160 (2004).

[11] I. N. Mishustin and J. I. Kapusta, Phys. Rev. Lett. **88**, 112501 (2002).

[12] V. K. Magas, L. P. Csernai, and D. Strottman, Nucl. Phys. **A712**, 167 (2002).

[13] Rainer J. Fries, Joseph I. Kapusta, and Yang Li, Nucl. Phys. **A774**, 961 (2006).

[14] Yu. B. Ivanov, I. N. Mishustin, and L. M. Satarov, Nucl. Phys. **A443**, 713 (1985).

[15] C. Y. Wong, *Introduction to High-Energy Heavy-Ion Collisions* (World Scientific, Singapore 1994).

[16] D. Kharzeev and M. Nardi, Phys. Lett. **B507**, 121 (2001).

[17] D. Kharzeev and E. Levin, Phys. Lett. **B523**, 79 (2001).

[18] M. A. Braun, F. del Moral, and C. Pajares, Phys. Rev. C **65**, 024907 (2002).

[19] I. N. Mishustin and K. A. Lyakhov, in preparation.

[20] J. D. Bjorken, Phys. Rev. D **27**, 140 (1983).

[21] L. M. Satarov, I. N. Mishustin, A. V. Merdeev, and H. Stöcker, Phys. Rev. C **75**, 024903 (2007).